Research Article

Ensiye Shabanlou, Babak Jaleh*, Saeid Azizian, and Kyong Yop Rhee*

Laser ablation and chemical vapor deposition to prepare a nanostructured PPy layer on the Ti surface

https://doi.org/10.1515/ntrev-2024-0055
received February 29, 2024; accepted June 13, 2024

Abstract: The deposition of polypyrrole (PPy) on a Ti surface is commonly employed to enhance the material's properties for different applications such as supercapacitors, biomedicine, and corrosion resistance. Instead of complex or costly polymerization procedures for the PPy synthesis on the Ti metal surface, we utilized the effect of a simple and inexpensive laser ablation of the Ti surface in the open-air environment to prepare a hydrophilic TiO_2 surface. In this condition, a thin PPy layer with remarkable nanostructures such as nanorings (~80 nm) and nanotubes (~245 nm) was deposited on a selective and desired pattern of ablated Ti areas through the chemical vapor deposition process using ferric chloride ($FeCl_3$) solution as a pyrrole oxidizer. Raman and X-ray photoelectron spectroscopy (XPS) analyses confirmed the PPy formation on the Ti surface. The creation of these nanostructures was due to the micro/nanomorphology of the ablated Ti substrate. Water contact angle (WCA) measurements indicated the hydrophobic behavior of the PPy/Ti surface by the aging effect after 24 weeks with the change of WCA from 20° to 116°. The change in the surface chemical composition upon adsorption of airborne organic compounds with the long-term storage of PPy/Ti surface in air was studied by the XPS test.

Keywords: titanium, polypyrrole, CVD synthesis, laser patterning, surface wettability

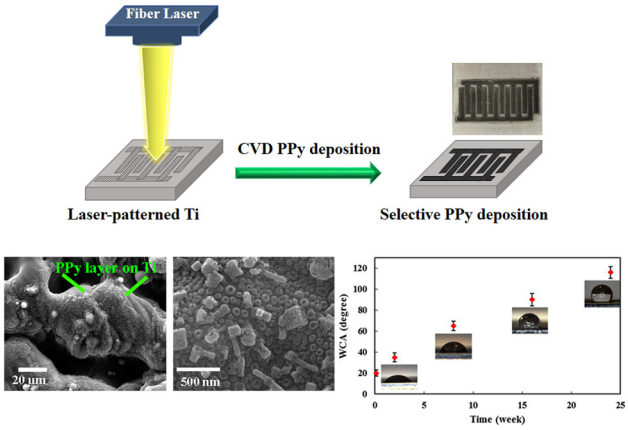

Graphical abstract

1 Introduction

Titanium (Ti) and its alloys have attracted a lot of attention for use in biomedical and industrial applications owing to their good corrosion resistance, excellent mechanical properties, and easy shapeability [1–5]. To improve the chemical, biological, and mechanical properties of Ti and its alloys, various techniques have been introduced, namely, thermal treatment [6], spraying [7,8], anodizing [9,10], polymerization [4,11], and laser techniques [12–17]. Among these methods, the polymerization of different polymers on Ti has been considered the suitable method for vast scientific studies [5]. Conducting polymers, due to their high stability, easy synthesis process, low cost, and high conductivity [18,19], are widely employed as promising materials in various areas like corrosion resistance [20,21], biomedical applications [18,22], polymer light-emitting diodes [23], thin-film transistors [24], supercapacitors [25–27], electromagnetic shielding [28], electro-chromic devices [29], molecular electronics [30], flexible electrodes [31], and sensor technology [32,33]. Polypyrrole (PPy) as a conductive polymer has been most extensively researched due to its special chemical and physical properties like good biocompatibility, fairly high conductivity, and novel optical and electrochemical properties [22,34,35]. PPy can be coated as a protective layer for different

* **Corresponding author: Babak Jaleh**, Department of Physics, Faculty of Science, Bu-Ali Sina University, Hamedan, 65174, Iran, e-mail: jaleh@basu.ac.ir
* **Corresponding author: Kyong Yop Rhee**, Department of Mechanical Engineering, Kyung Hee University, 17104, Yongin, Republic of Korea, e-mail: rheeky@khu.ac.kr
Ensiye Shabanlou: Department of Physics, Faculty of Science, Bu-Ali Sina University, Hamedan, 65174, Iran
Saeid Azizian: Department of Physical Chemistry, Faculty of Chemistry and Petroleum Sciences, Bu-Ali Sina University, Hamedan, Iran

materials to enhance their properties in various applications through chemical oxidative polymerization, electrochemical polymerization, or vapor-phase polymerization methods [36–39]. The high stability of PPy coating over Ti helps to prevent the electron exchange between the metal and the adsorbed biological species [40], which indicates excellent corrosion resistance behavior [32]. Compared to other heterocyclic monomers, pyrrole (Py) has a lower oxidation potential, which may help to form a PPy film on active metals easily and provide anti-corrosion properties. However, synthesizing PPy films on oxidizable metals like Fe, Zn, Al, and Ti and their alloys with good adhesion is more difficult than on other metals [41–43]. The force of adhesion between the PPy deposition and the oxidizable metals is poor, which seriously limits their application [42,43]. Furthermore, despite all PPy advantages, it is brittle in nature [42,44]. Although significant progress has been made to improve the adhesion force between PPy and the aforementioned metals, researchers still desire to find effective methods for solving these issues [43,45]. Incorporating a natural polymer such as chitosan into the matrix of PPy can be a good solution to overcome the problem of PPy's brittleness [42]. Furthermore, a suitable material (like dopamine) can be used as an interlayer between the PPy film and the Ti substrate for improving the adhesion force [43,45], and in another report PPy–polyethylene glycol composite films were used as an insulting polymer to synthesize PPy on Ti by the electrochemical method [41]. Based on our library information, PPy was often deposited on Ti by electrochemical polymerization assisted by different Ti modification processes for biological and anti-corrosion applications. Table 1 presents a brief information on previous studies. However, the electrochemical polymerization method requires electric power supply, different electrode materials, supporting electrolyte solution, and solvents which are complex and expensive [46]. Moreover, chemical polymerization has the limitations of needing more purification and further characterization for their confirmation. Electrochemical polymerization has the disadvantages of low yield and poor solubility of the product, the former making the method unsuitable for large-scale and selective deposition of polymers [46]. Hence, to carry out PPy synthesis on Ti with good adherence, it is better to try another method such as chemical vapor deposition (CVD). In the CVD method, a monomer, *e.g.*, Py using oxidizing agents like ammonium persulfate and ferric chloride ($FeCl_3$) directly polymerizes uniformly on the substrate surface in a one-step process under dry and vacuum conditions without any subsequent curing steps [47]. The CVD advantages like thickness control, conformality, selective layer deposition, and functional group retention have been more emphasized [48]. Despite these advantages, CVD has a limited dispersion of the oxidant on the Ti substrate for the formation of a

Table 1: Previous studies on PPy coating on Ti/Ti alloys by various treatments

Resulting product	PPy synthesis method	Substrate	Application	Ref.
PPy-Ti_xO_y	Electropolymerization	Chemically pre-oxidized Ti	—	[90]
Ti (or Ti-Al-V)-PPy	Electropolymerization	Ti and Ti-Al-V	—	[91]
Ti-PPy	Electropolymerization	Ti	Corrosion resistance	[34]
Ti-PPy	Electropolymerization	Ti modified with 1-pyrrolyl-10-decylammonium phosphonate (PyDPA)	—	[92]
p-Toluenesulfonate-PPy film on TiO_2 nanotubes/Ti	Electropolymerization	TiO_2 nanotubes/Ti foil	Sodium ion battery	[93]
PPy/chitosan composite coating on Ti	Electropolymerization	Ti	Corrosion resistance and biocompatibility	[42]
Biotin-doped polypyrrole titanium (Bio-PPy-Ti)	Electropolymerization	Ti	Osteoinductive ability	[94]
PPy/graphene oxide on Ti	Electropolymerization	Ti	Biomedical implants	[95]
PPy and N-doped reduced graphene oxide (NrGO) on Ti	Electropolymerization	Mixed metal oxide-coated Ti	Hydrogen and oxygen generations	[96]
PPy and NrGO on Ti	Electropolymerization	Mixed metal oxide-coated Ti	Water splitting	[97]
PPy/modified plasma electrolytic oxidation ion (PEO) Ti	Electropolymerization	Modified Ti with PEO	Cell biocompatibility	[98]
PPy–silver nanoparticles (PPy-AgNPs) on porous Ti	Electropolymerization	Macroporous Ti substrates created with a space-holder technique	Corrosion resistance and antibacterial behavior	[99]
PPy-coated Ti	Electropolymerization	Ti	Support osseointegration	[4]

homogenous polymer layer [36]. Therefore, a dispersing agent or surface treatment process should be used to spread oxidants uniformly during the CVD polymerization process [36]. To overcome this challenge, it is possible to treat the surface by influencing the Ti morphology and its structure before depositing PPy. Micro- and nanostructures have been created on surfaces using different techniques, including electron beam, photolithography, particle beam, ion beam, X-ray, radio frequency magnetron sputtering, and mechanical methods [49–53]. In recent years, laser-based technologies have gained significant attention for surface treatment [49,54,55]. The laser ablation method without needing a complex process and extra chemical material is a one-step, easy, green, low-cost, as well as controllable laser process by adjusting the laser parameters [56–60]. The improvement of surface properties and formation of new structures with laser approaches such as TiN, TiC, and TiO_2 of Ti and its alloys have been studied by many researchers [13–16,61,62]. In the laser ablation process, the wetting state of a solid surface is significantly influenced by changing the surface microstructure such as roughness and its chemical composition [63]. The pristine Ti metal surface possesses partial hydrophilicity, with a water contact angle (WCA) of around 70°. To achieve full superhydrophilicity, laser ablation can be employed on Ti [13,64], which resulted in the formation of micro/nanostructures on the metal's surface through material re-deposition and re-solidification. The wettability properties of metal surfaces can be adjusted by altering the surface roughness and generating new microstructures [63,65]. In line with Wenzel's model [66], enhancing surface roughness improves the surface wettability. Laser scanning paths created cavity-like patterns on the metal surfaces, promoting the uniform spreading of water across the surface [64]. Additionally, during the laser modification process, molten material generated from the thermal treatment could react with airborne oxygen, leading to surface oxidation and an increase in total surface energy (γ) [64]. This increase results from various types of intermolecular forces, including non-dispersive and dispersive components ($\gamma = \gamma^{P} + \gamma^{d}$) [64,67]. The polar or non-dispersive (γ^{P}) and dispersive (γ^{d}) components play crucial roles in determining the hydrophilic and hydrophobic behavior of solid metal surfaces, respectively [64,67]. In the study of Razi *et al.* [64], it was demonstrated that melting the Ti surface during the laser ablation process increased the surface oxygen content, surface activation, and γ^{P} as the polar component, resulting in superhydrophilic behavior of the Ti surface. Inspired by this issue, this study presents an innovative approach for the selective deposition of a PPy layer with a desired pattern and good adherence on Ti surfaces using a fiber laser device and CVD techniques. The superhydrophilic behavior of ablated Ti helps the aqueous solution of $FeCl_3$ (oxidizing agent) to completely wet the irradiated areas and synthesize the PPy layer as selective and desirable arrays with a thickness of about 530 nm by the CVD method. Raman spectroscopy and X-ray photoelectron spectroscopy (XPS) confirmed the successful formation of PPy on the Ti surface. Field emission scanning electron microscopy (FESEM) images revealed the formation of a thin PPy layer in (nano)ring and (nano)tube structures at different CVD times. This kind of PPy morphology was created with the influence of pre-laser treatment of the Ti substrate. In the classical preparation method of PPy, it was often grown in cauliflower-like structures with spherical or globular grains [68,69]. This morphology is attributed to the difficulty in dopant intercalation in the irregular structure of polymer chains reported in the literature [70]. The fabrication of nanostructured PPy attracted much attention over bulk-structured PPy to potentially improve its applications. The study also includes the effect of aging on the wettability of PPy/Ti samples using WCA measurements and XPS analysis, revealing changes in polar and nonpolar components as significant factors in surface wettability. Despite the inherent hydrophilicity of PPy because of the presence of amine groups, this study shows a hydrophobic surface with a WCA of approximately 116°. Generally, with the synergistic effect of the laser ablation process and the CVD method, the PPy nanostructure was coated on the Ti surface, which can enhance the performance of PPy/Ti material applications as a promising avenue for future research.

2 Materials and methods

To fabricate PPy/Ti samples, we used the Ti metal sheet (purity: 98.90%; thickness: 0.6 mm; Grade 2) from LOTERIOS, a TIMET Co., and Pyrrole, catalog No. M8074920100 and solid $FeCl_3$ from Merck. The Ti metal sheet was laser-cut into 17 × 17 mm^2 pieces. Then, they were ground with SiC papers and subsequently washed using an ultrasonic device with distilled water. Also, a 1 M aqueous $FeCl_3$ solution was prepared as the oxidizing agent. Among the samples, one of them was applied as a reference Ti, while the three others were selected for laser ablation and PPy deposition. To achieve complete superhydrophilic behavior of the Ti surfaces, they were irradiated in an air environment using a fiber laser (RFL-P30Q, 1,064 nm; maximum power: 30 W; pulse width: 100 ns). In this experiment, the distance of the laser scanning path in the x direction was set at 50 μm, and laser parameters, including the scanning speed, power, fluence, and repetition rate, were adjusted to 200 mm/s, 27 W, 68 J/cm^2, and 20 kHz, respectively. Figure 1 illustrates the surface wetting behavior of the Ti surface before (Figure 1a: [I–IV]) and immediately after the laser

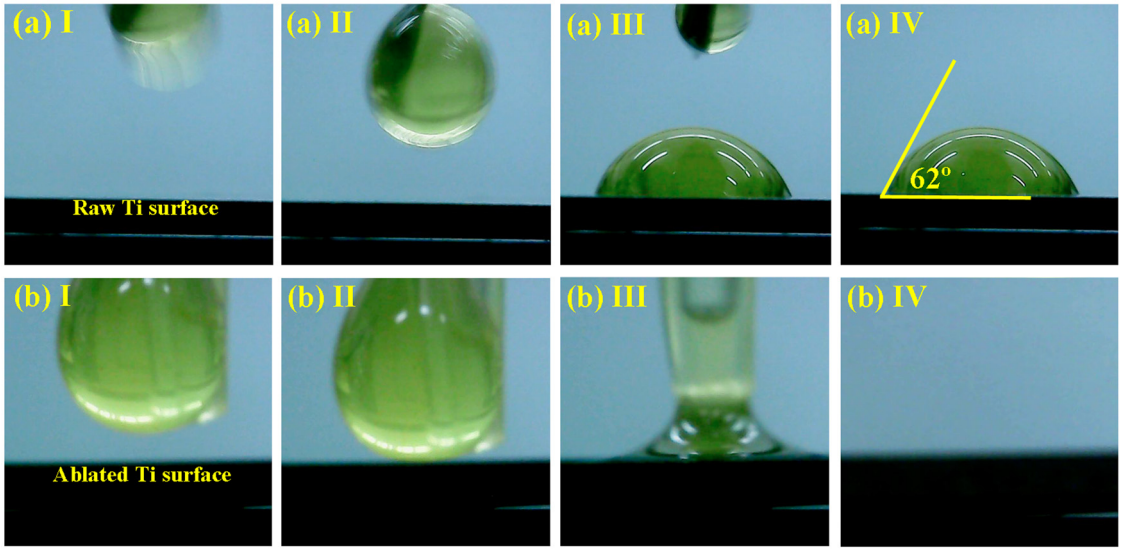

Figure 1: Wetting behavior of the Ti surface before (a) and after (b) the laser ablation process.

ablation process (Figure 1b: [I–IV]) tested with a 5 µl droplet of $FeCl_3$ solution. As is shown, the $FeCl_3$ solution was evenly spread over the ablated surface immediately after the laser treatment. To dry the $FeCl_3$ solution on the ablated Ti surfaces, they were left under ambient conditions for approximately 30 min. Following that, the ablated samples were individually placed in a sealed chamber containing a liquid Py monomer. Vapor-phase deposition of PPy on the irradiated Ti surfaces was conducted in the absence of light at room temperature for durations of 4, 8, and 12 h, referred to as S4, S8, and S12, respectively. Various methods were employed for the identification and analysis of the resulting samples. The sample structures, before and after PPy deposition, were assessed using a micro-Teksan Raman device (Takram P50C0R10; laser beam wavelength: 532 nm) in the range of 100–2,000 cm^{-1}. The XPS test was applied on the PPy/Ti sample using XPS devices (250Xi and Bestec GmbH, Germany). The wettability behavior of the PPy/Ti surfaces was studied by measuring the WCA. The morphology of the samples' surfaces was examined using SEM instruments (JEOL-JSM-840A and FESEM Mv2300-TESCAN).

3 Results and discussion

3.1 Characterization analyses

PPy deposition on Ti surfaces was successfully achieved through straightforward and cost-effective laser and CVD methods. Following the vapor deposition of PPy on Ti surfaces, they exhibited a complete transformation to a black color, characteristic of PPy. In Figure 2(a–d), optical images of ablated Ti, S4, S8, and S12 are presented. These images reveal that PPy was deposited on the laser-ablated areas of the Ti surface. The schematic of PPy deposition on the ablated Ti surface is presented in Figure 3.

3.1.1 Raman spectroscopy

Raman characterization was performed to analyze the ablated Ti and S4 as a PPy/Ti sample in the spectral range

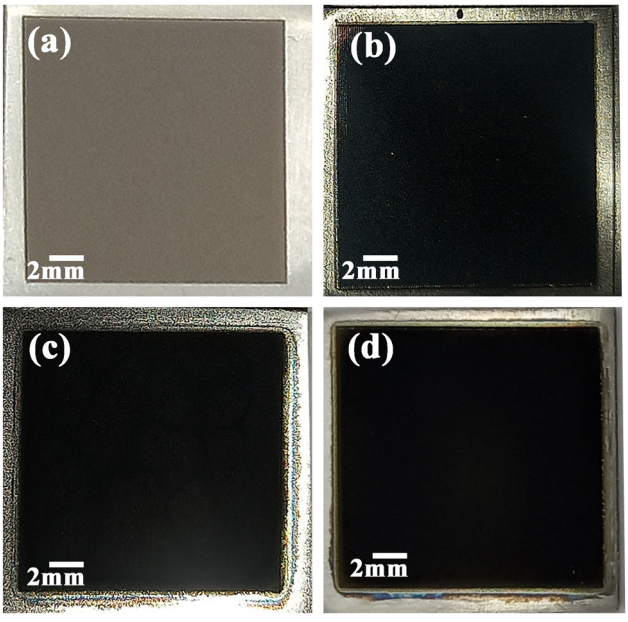

Figure 2: Optical images of laser-ablated Ti (a), S4 (b), S8 (c), and S12 (d) samples.

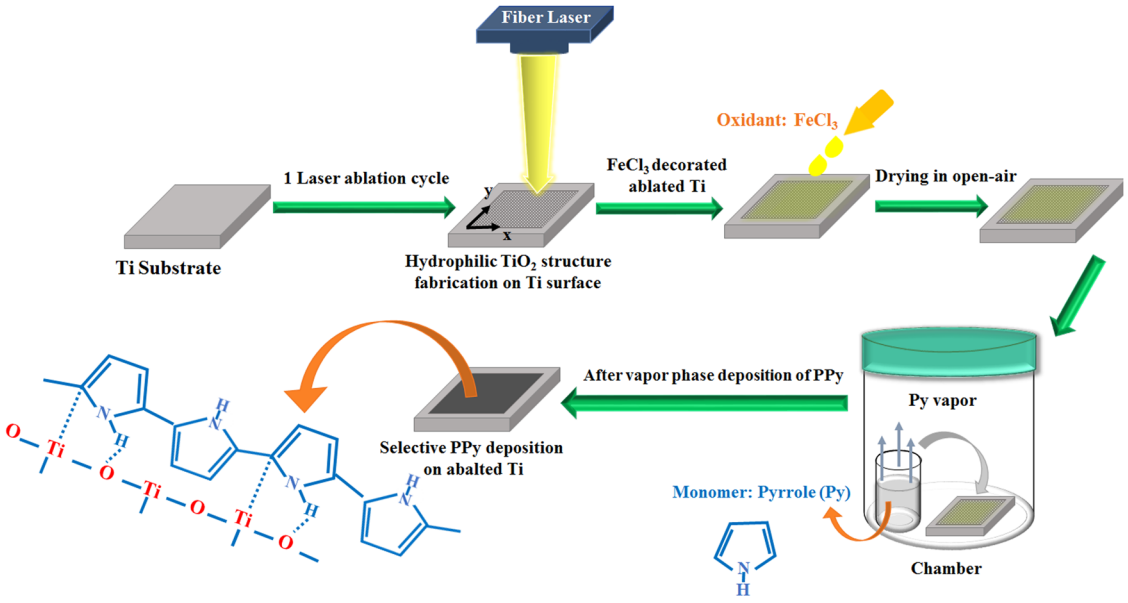

Figure 3: Schematic of the PPy deposition process on the ablated Ti target.

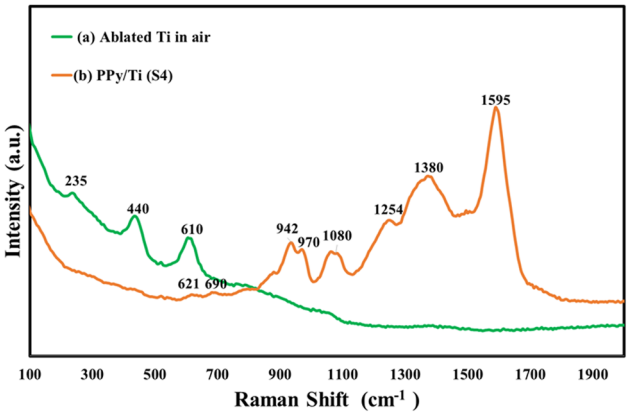

Figure 4: Raman spectra of ablated Ti in air (a) and PPy/Ti (b).

of 100–2,000 cm^{-1}. The two patterns (a) and (b) in Figure 4 correspond to the Raman spectra of irradiated Ti in ambient air and the PPy/Ti (S4) sample, respectively. In the Raman spectrum of ablated Ti (a), two characteristic peaks are observed at almost 440 and 610 cm^{-1}, attributed to E_g and $A1_g$ symmetry species of rutile TiO_2, respectively [71]. Additionally, another peak is located at about 235 cm^{-1} in the Raman spectrum of ablated Ti, attributed to the second-order or two-phonon Raman scattering process [71]. The generation of the TiO_2 structure can be ascribed to the presence of oxygen molecules (O_2) in the air, which can participate in chemical reactions with plasma plume species such as Ti atoms generated during the ablation process, resulting in the formation of Ti oxide bonds [15,72,73]. The Raman spectrum of the PPy/Ti sample (Figure 4b) displays different Raman peaks between 620 and 1,609 cm^{-1}, matching with those of the PPy Raman spectrum [74–76]. The two peaks that appeared at about 620 and 690 cm^{-1} corresponded to C–C ring torsional and C–H wagging bonds. respectively [75]. The Raman spectrum of PPy/Ti (Figure 4b) displays absorption peaks at approximately 1,595 and 1,380 cm^{-1}. These peaks belong to the stretching vibrations of C=C and C–N bonds, respectively [32,77]. Additionally, the Raman scattering is primarily determined by the peak at approximately 1,254 cm^{-1} attributed to the C–H in-plane bending vibration [75,77]. Two other peaks that appeared at about 1,080 and 942 cm^{-1} are ascribed to the deformation vibrations of C–H and C–C rings, respectively [75,77]. Furthermore, the peak at about 970 cm^{-1} of PPy/Ti Raman spectrum belonged to the C–C ring deformation in Py [32,75]. These results prove that PPy has been successfully deposited on Ti metal, so that the Raman peaks corresponding to TiO_2 did not appear anymore which concludes that the PPy successfully covered the Ti surface.

3.1.2 XPS investigation

The chemical composition information of the PPy/Ti (S4) surface after about 4 weeks was studied in detail by the XPS test. The survey spectrum of the PPy/Ti surface is presented in Figure 5a. It demonstrates that the PPy-coated Ti surface consists of nitrogen (N), oxygen (O), and carbon (C) elements that originated from PPy. The atomic percentages of N, C, O, and Ti in the S4 sample's surface are 12.68, 64.11,

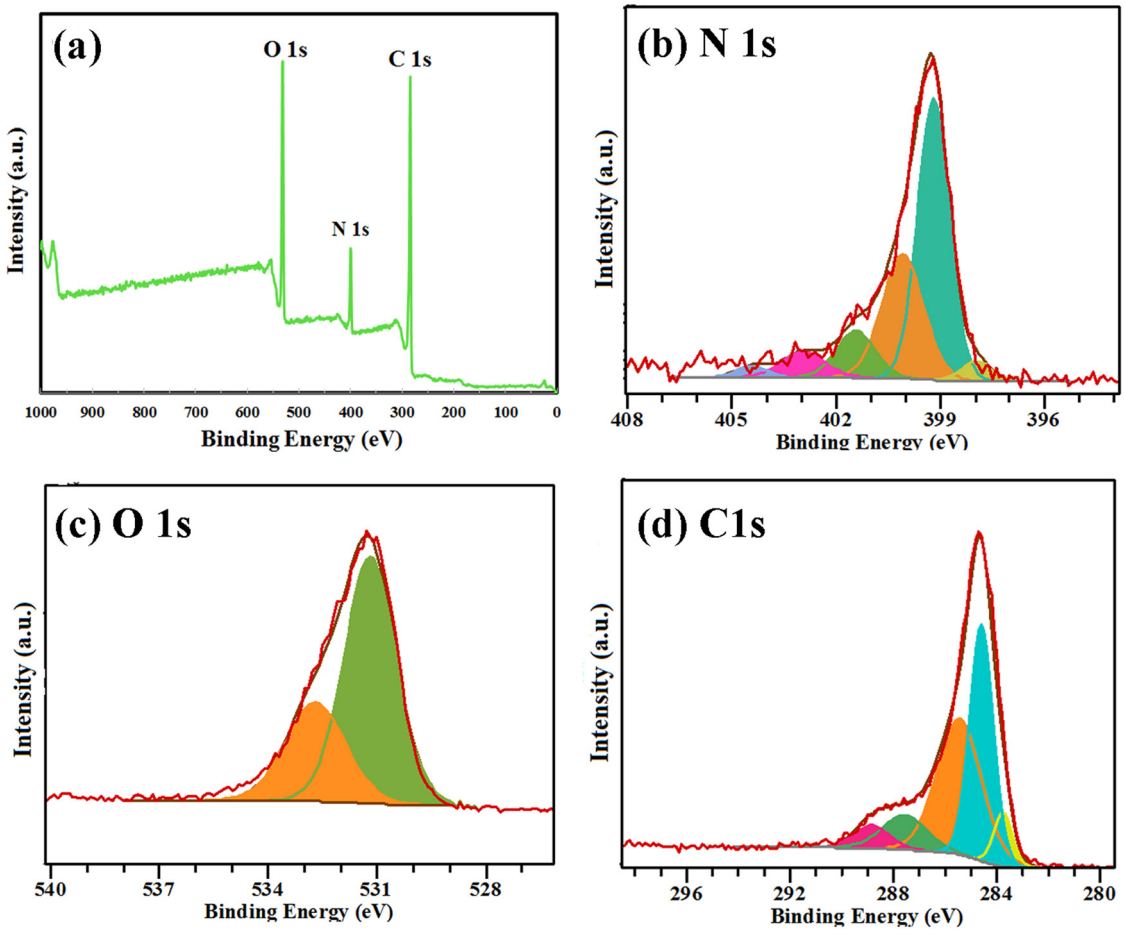

Figure 5: XPS full survey spectrum (a) and XPS peak fitting of N 1s (b), O 1s (c), and C 1s (d) of the PPy/Ti (S4 sample) surface.

22.58, and 0.63%, respectively. Here, the Ti surface was thoroughly covered with PPy, so the Ti element was detected by the XPS test in very small quantities. In the following, the de-convoluted XPS line of PPy/Ti compounds was perused, and its results are given in Figure 5(b–d). N 1s XPS spectrum (Figure 5b) is de-convoluted by five peaks at about 397.9, 399.2, 400.1, 401.4, and 402.8 eV as =N–/C=N [37,75,78], neutral amine nitrogen –NH–/C–N [78,79], $–NH^+$, $C–N^+$, and $C=N^+$, respectively [75,78–80]. Another peak appeared at about 404.4 eV as $=N–H^+$ [80]. As seen in Figure 5c, two distinct O 1s peaks at the binding energies of 531.1 and 532.7 eV belong to C=O and C–O bonds, respectively [78,81]. Also, five C 1s peaks were found in its region spectrum (Figure 5d). The most intense peak at 284.6 eV is related to α carbon (C_α) atoms in the Py ring in which C atom bonds to a functional group leading to form C–C or C=C bonds [75,79]. The component at 283.7 eV is for β carbon (C_β) atoms which the C atoms have not bonded with the functional group [75,79]. The binding energy at about 285.4 eV is related to the presence of C–N, C–O, and $C–N^+$ components [75,79]. The presence of C=N, C=O, and $C=N^+$ components was confirmed with the located peak at 287.6 eV [75,78,79]. The peak at approximately 288.4 eV is ascribed to C–O and C=O bonds, indicating the numerous oxygen-containing functional groups of PPy [80,82]. The parameters of fitting components, namely, the peak position, peak area (%), and full-width-at-half-maximum (FWHM), are given in Table 2. According to the literature [83,84], TiO_2 has strong bonds with H and C atoms of Py such that the O atoms of TiO_2 interact with N-bonded H atoms of Py through strong hydrogen bonding (mostly covalent) and Ti has a strong electrostatic type of bonding with the C. Due to the thinness of the PPy layer, the XPS analysis could not measure the binding energy. In the study of Ullah [83], the inter-molecular interaction in PPy/TiO_2 was investigated using density functional theory calculations, and the inter-molecular interaction energy obtained was about −28 to −45 kcal/mol, which confirmed the strong covalent type of bonding between Py and TiO_2.

Table 2: XPS peak fitting parameters of N 1s, O 1s, and C 1s which are shown in Figure 5

Peak	Component	E_b (eV)	FWHM (eV)	Area (%)
N 1s	═N–/C═N	397.9	1.00	3.40
N 1s	–NH–/C–N	399.2	1.05	49.69
N 1s	$–NH^+$	400.1	1.39	28.85
N 1s	$C–N^+$	401.4	1.28	10.11
N 1s	$C═N^+$	402.8	1.44	6.14
N 1s	$═N–H^+$	404.4	1.00	1.81
O 1s	C═O	531.1	1.67	68.51
O 1s	C–O	532.7	1.91	31.49
C 1s	C_β	283.7	0.84	06.70
C 1s	C_α (C–C/C═C)	284.6	1.07	37.35
C 1s	$C–N/C–O/C–N^+$	285.4	2.01	40.25
C 1s	$C═N/C═O/C═N^+$	287.6	2.04	10.33
C 1s	C–O/O═C	288.4	1.58	05.37

3.1.3 FESEM/SEM images

The morphology of the irradiated Ti surface before the process of PPy deposition is shown in Figure 6a(I–III) at different magnifications. The effect of laser ablation on the Ti surface is observable in the 6a(I) image. The ordered pores and cavities due to the horizontal lines of the laser scanning cycle were created on the surface of Ti [85]. The result is a change in the Ti surface's roughness and porosity, which has significant effects on its wetting behavior [64,85]. In FESEM images of Figure 6a(I and II), some particles can be seen on the Ti surface which are generated because of the laser ablation mechanism. The Ti surface reaches its melting point due to the laser thermal effect and creates a plasma plume on the irradiated area; the

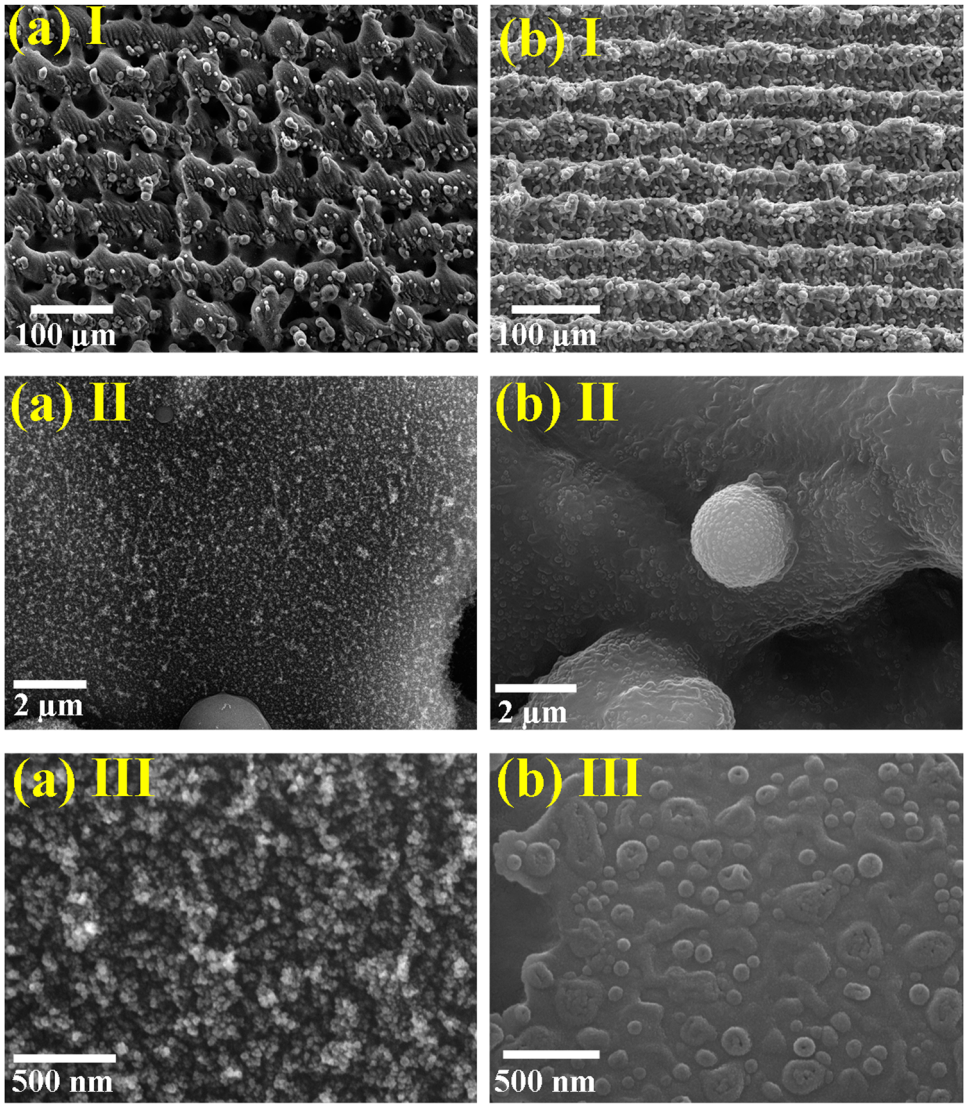

Figure 6: FESEM images of the irradiated Ti sample before (a [I–III]) and after (b [I–III]) PPy deposition on it of S4.

explosive melting occurs and the nanodroplets of ionized matter (free atoms, ions, and clusters) are ejected from Ti, and these nanodroplets can fabricate (sub)micrometric particles and finally solidify on the ablated surface [86]. As seen in Figure 6b(I–III) of the S4 sample, after PPy deposition, the irradiated Ti surface and particles were covered with a compact and uniform PPy layer with numerous nanorings. In the conventional preparation method of PPy, it was often grown in cauliflower-like structures with spherical or globular grains [68,69]. This morphology is attributed to the difficulty in dopant intercalation in the irregular structure of polymer chains reported in the literature [70]. In the present work, the PPy layer was grown on the Ti surface with different nanostructures. Figure 7(a–d) illustrates the FESEM images of S8 at different magnifications. As found in FESEM images of S8, structures like nanorings (donuts) are uniformly formed all over the Ti surface with an average size of about 80 nm. In addition to (nano)rings, the PPy was also fabricated as (nano)tubes and cubic-like structures on the S8 surface. The average length of (nano) tubes was calculated at about 245 nm. In contrast to the methods (like soft micellar or hard physical template methods, templateless, and electrochemical techniques) that have been used to make different PPy nanostructures [87], our tactic is very simple and of low cost resulting in PPy deposition on the Ti surface. The morphology of the PPy structure of sample S12 is almost the same as S8 (Figure S1). By increasing the deposition time up to 8 h, nanocubic and nanotube structures of PPy grew on the ablated Ti surface because Py has more opportunities to be absorbed on the Ti surface impregnated with the $FeCl_3$ oxidant, although the amount of nanocubes and nanotubes were less compared to the nanorings. There are no tangible differences in the morphology of samples S8 and S12. It is probably due to the ability of the oxidant ($FeCl_3$) to absorb the Py monomer. To investigate the reason for forming this kind of nanostructure, SEM images were taken from the $FeCl_3$ solution-impregnated Ti surface, which are presented in Figure S2(a–c). From these images, it can be concluded that the (nano)tubes, (nano) rings, and cube-like structures are not related to $FeCl_3$ crystals. On the other hand, to find whether these PPy nanostructures are related to the ablating Ti substrate or not, we chose a raw Ti sample without any laser processing, and in the CVD conditions of sample S8, the PPy was formed in a scattered and low-quality manner on Ti. According to its SEM images (Figure S2(d–f)), we did not see any trace of the PPy (nano)ring or (nano)tube formation. Hence, it can be said that the morphology of PPy (nano)structures was

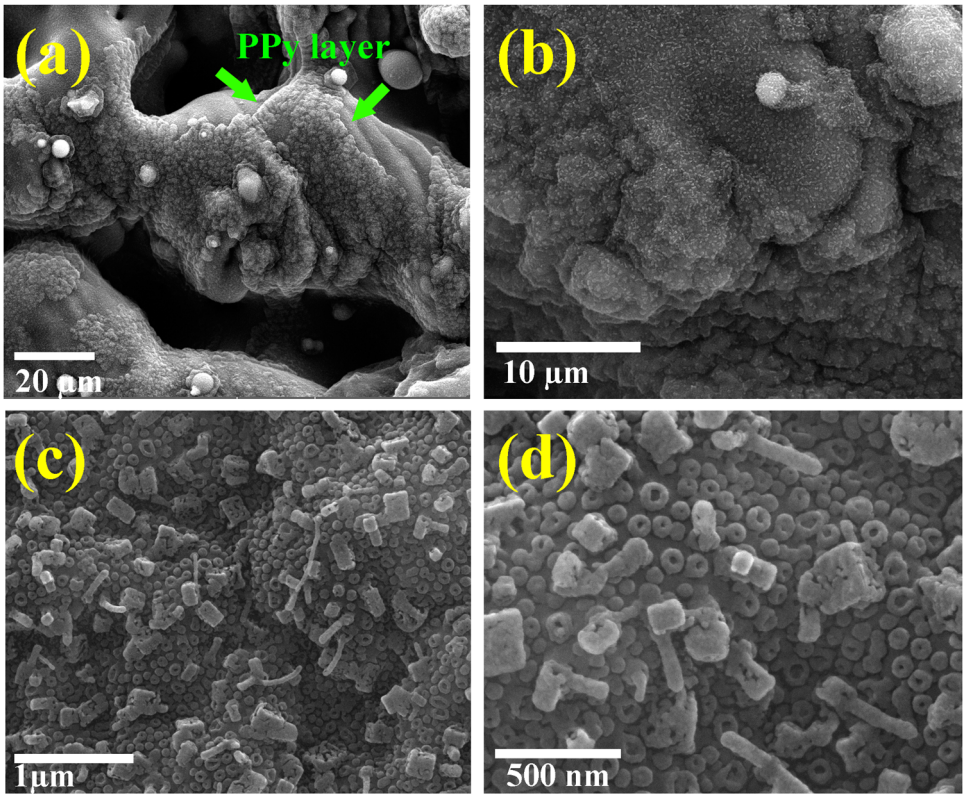

Figure 7: FESEM images of the surface of sample S8 at different magnifications (a–d).

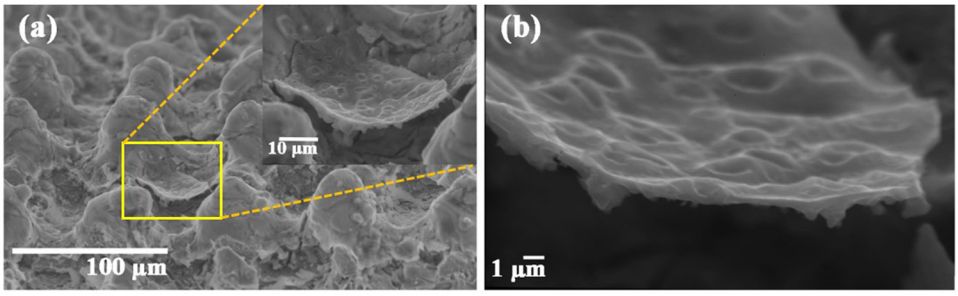

Figure 8: SEM images of separated PPy layer from the S8 surface with scale bars of 100 µm (a) and 1 µm (b).

affected by micro/nanoporous structures and nanodroplets of the laser-ablated Ti as the PPy substrate.

For investigating the thickness of PPy films and their cross-section morphology, we tried to take the FESEM images of the samples. Figure S3(a–c) illustrates the cross-sectional images of sample S4. As can be seen, the part of Ti thickness that has been exposed to the laser beam is visible, and it has a thickness of about 26 µm. However, the thickness of the thin PPy film cannot be recognized due to the porous morphology of the ablated surfaces. Also, this condition was for S8 and S12 samples. With more and more investigation, at last, we could find a small part of the PPy layer which was separated from the ablated Ti surface of S8, as given in Figure 8(a and b). The average thickness of the PPy layer from S8 was calculated to be about 530 nm.

3.2 Selective surface patterning

Inspired by the laser ablation technique and its effect on enhancing the hydrophilic behavior of Ti, micropatterns are created on the Ti surface. At first, some micropatterns which are mainly used in electrodes in various applications such as sensors, biomedicine, and electrocatalysts were designed by a fiber laser device and then the Ti surface was selectively irradiated through the pattern. As can be seen in the optical images of Figure 9, the micropattern was formed with a clean and accurate method, so that PPy just covered the irradiated pattern. The irradiated parts of Ti became hydrophilic as a selective-wetting surface which these areas could just wet with $FeCl_3$ solution. Therefore, after the deposition of PPy on the patterned Ti surface, a selective-PPy surface with neat and clean arrays was

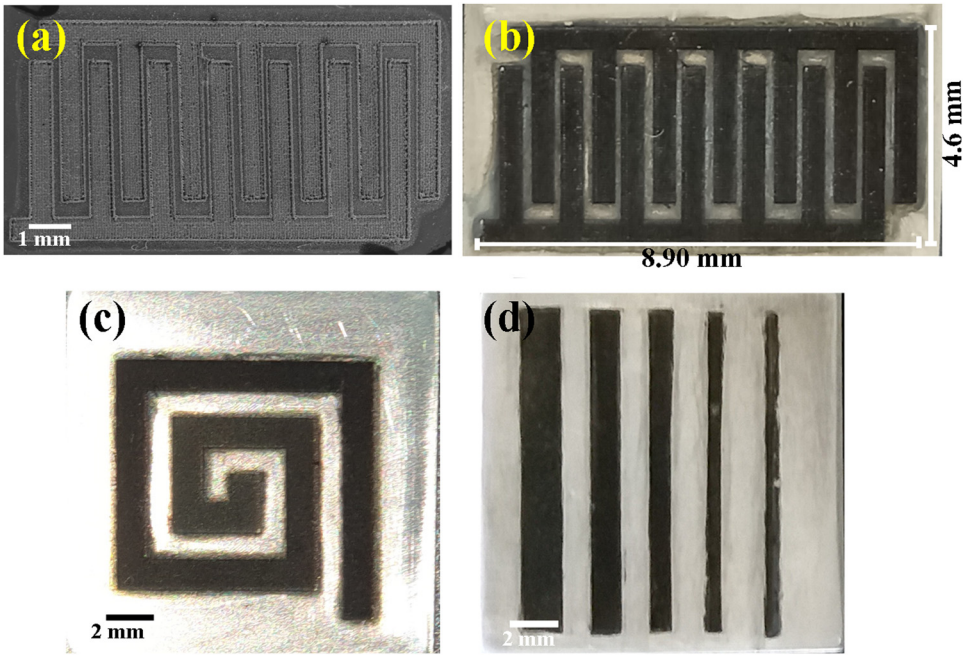

Figure 9: SEM (a) and optical (b) images of selective-PPy surface patterning like interdigitated electrode arrays. Optical images of different neat and clean arrays from the patterned-PPy/Ti surface (c) and (d).

obtained on a micro scale. This method is presented for the first time with easier and inexpensive processes compared to other polymerized electrode patterning techniques.

3.3 Surface wettability

In the present study, the surface wettability of raw Ti, S4, S8, and S12 samples was measured with the WCA. The surface of pristine Ti metal was found to be partially hydrophilic with a WCA of about 62°. As explained in Section 1, immediately after performing laser ablation, the Ti surface completely became superhydrophilic and then the PPy could be synthesized on the surface of irradiated Ti. After coating PPy on irradiated Ti surfaces, the effect of aging on the wettability behavior of S4, S8, and S12 surfaces was investigated, and it was found that all samples became hydrophobic over time. After 24 weeks, their WCAs were about 110–120°, which was not very different. The morphologies of samples were almost similar with numerous micro/nanostructures, so they did not have much effect on the wettability. Therefore, among the studied samples, S4 was chosen for the wettability study at time intervals of 2, 8, 16, and 24 weeks and XPS and Raman analyses were conducted for the S4 sample. Immediately after PPy deposition on the Ti surface, its WCA was about 20°. Its hydrophobic behavior increased due to the aging effect, with the WCAs of about 35°, 65°, 90°, and 116° in 2, 8, 16, and 24 weeks, respectively (Figure 10). Considering that surface wettability can be influenced by surface morphology, the FESEM images, immediately after PPy deposition and over 24 weeks, were taken on S4. As given in Figure S4, the morphology of the S4 surface did not significantly change by the aging effect, hence it was concluded that the changes in wetting behavior over time are not related to the surface morphology. So, the chemical

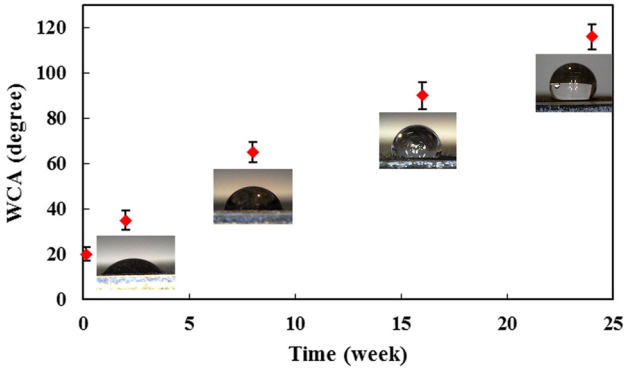

Figure 10: Variation in the WCA of S4 through the aging effect.

Table 3: XPS composition (At. %) of S4 (after 4 weeks of PPy deposition) and S4* (after 24 weeks of PPy deposition)

Sample	Composition (At. %)			
	Ti 2p	C 1s	O 1s	N 1s
PPy/Ti (S4)	0.63	64.11	22.58	12.68
PPy/Ti (S4*)	0.68	69.86	16.68	12.78

composition of the surface as an important factor for changing wettability was studied [88]. The XPS analysis of S4 was performed on its surface after 24 weeks, which was named S4* to confirm the chemical composition's effect on surface wettability behavior. The change in the amount of O and C was studied in S4* and S4. Table 3 shows comparison results of the composition values of S4* and S4 by XPS analysis. S4 surface indicated C and O contents of 64.11 and 22.58%, respectively, and the C and O contents of S4* changed to 69.86 and 16.68%, respectively. The oxygen-to-carbon (O/C) ratio is clearly the reason for the change in the wetting state of surfaces [89]. The O/C atomic percentage ratio decreases with the aging effect and causes the hydrophobic behavior. Therefore, in this study, decreasing the O/C ratio is one of the reasons for the hydrophobicity of the PPy/Ti sample, and its value reaches from 0.35 to 0.24 after 24 weeks. Aging oxidation has an important effect on the wettability behavior of hydrated structures [63]. Upon oxidation of the surface, the tendency of micro/nanostructures of the laser-treated surface to various chemical reactions increases. The oxidation process can increase the surface activity for the adsorption of air contaminants because of the creation of different functional groups [64]. By keeping the formed micro/nanostructures in environmental conditions for a long time, the adsorption of airborne organic compounds and non-polar factors occurs which causes the surface energy reduction [64,85]. In this regard, the polar and non-polar functional groups of C 1s in S4* were investigated and compared with S4. The polarity of surfaces is an effective factor in the wetting state. Low or non-polarity leads to hydrophobic

Table 4: C 1s and O 1s components (At. %) of S4 (after 4 weeks of PPy deposition) and S4* (after 24 weeks of PPy deposition)

Sample	C 1s (%)					O 1s (%)	
	C_α (C–C/ C=C)	C_β	C–N/ C–O/ $C–N^+$	C=N/ C=O/ $C=N^+$	C–O/ O=C	C=O	C–O
S4	37.35	06.70	40.25	10.33	05.37	68.51	31.49
S4*	53.64	18.16	14.07	10.62	3.51	48.78	51.22

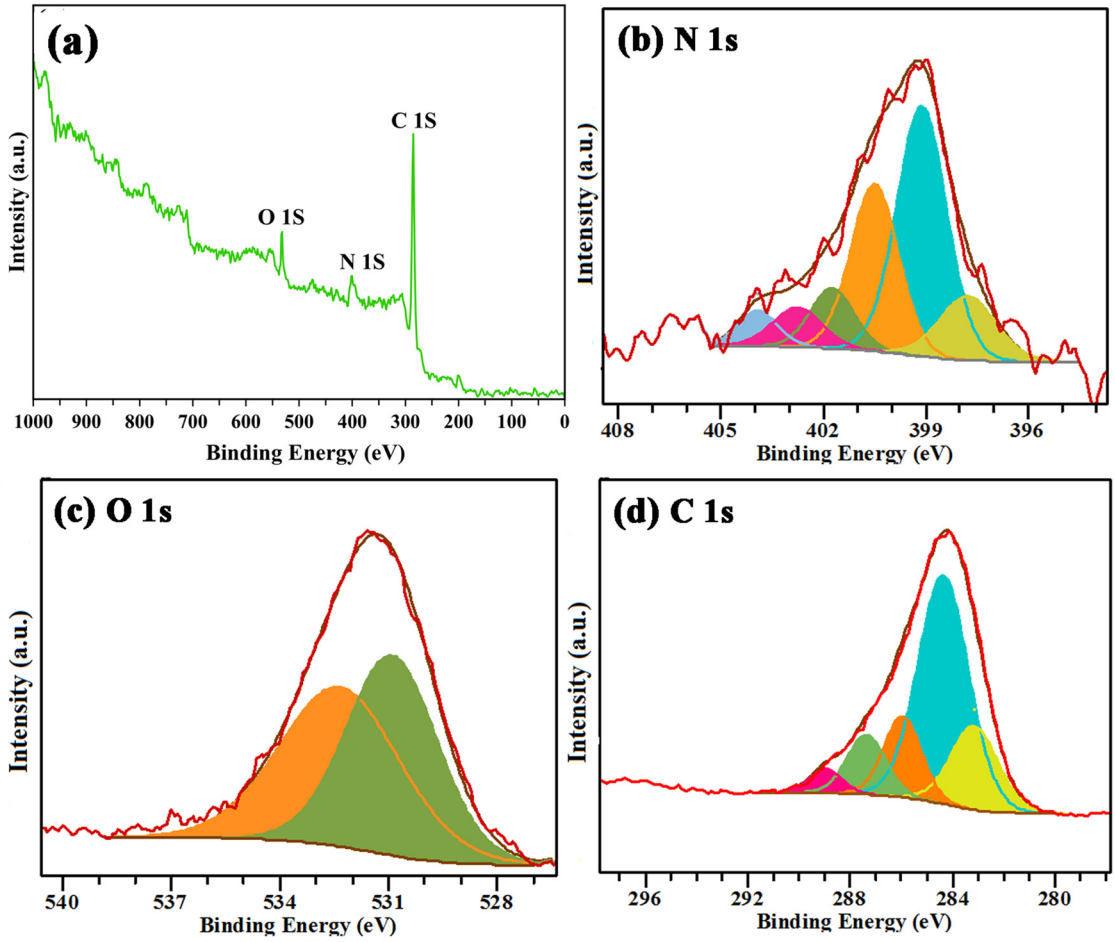

Figure 11: XPS full survey spectrum (a) and XPS peak fitting of N 1s (b), O 1s (c), and C 1s (d) of the S4* surface.

behavior, whereas high polarity causes the hydrophilic behavior of solid surfaces [66,85]. The amount of non-polar moieties (percentage) as a hydrophobic factor in S4* is more than that in S4 and leads to a hydrophobic surface. Their detailed results are presented in Table 4. Carbon accumulation on the surface plays an essential part in surfaces' hydrophobic behavior. In this regard, the polar and non-polar functional groups of C 1s in S4* were investigated and compared with those of S4. Polar groups of C 1s are carbonyl bonds (C═O), carbon–oxygen bonds (C–O), C–N, C–N^+, C═N, and C═N^+, while non-polar moieties include C_α (C–C/C═C) and C_β. The amount of non-polar moieties (percentage) as a hydrophobic factor in S4* is more than that in S4 and leads to a hydrophobic surface (Table 4). Furthermore, the functional groups of O 1s were investigated. The XPS survey spectrum and characteristic N 1s, O 1s, and C 1s spectra of S4* are displayed in Figure 11(a–d).

4 Conclusions

In summary, for the first time, the selective-PPy deposition on the Ti surface has been successfully performed *via* a simple laser treatment approach and CVD methods without requirement of a complicated chemical process and extra materials. The laser ablation process having influence on the Ti wettability behavior and producing superhydrophilic micro/nanostructures on the Ti surface could provide an ideal condition to wet the irradiated area by the $FeCl_3$ solution as the oxidizing agent of Py monomer. Hence, the PPy layer can only be deposited on the ablated part of Ti with CVD technique. The Raman and XPS spectra as well as FESEM images indicated that the thin PPy layer formation occurred with special nanorings and nanotubes. We also indicated that PPy can be deposited on desirable microarrays on Ti. The wetting behavior of the PPy/Ti

sample was studied over time, and it was concluded that the PPy/Ti surface became hydrophobic after 24 weeks with a WCA of about 116°. Considering that the surface morphology of the sample has no significant change over time, the surface chemical composition has probably changed the surface wettability. According to XPS analysis, the amount of non-polar compounds as a hydrophobic factor increased on the surface of samples with the aging effect due to the adsorption of airborne carbon compounds by micro/nanostructures of PPy and irradiated Ti surface. Overall, laser ablation, in addition to providing the PPy deposition path in desired designs on Ti surfaces, causes the formation of a new PPy structure on the nanoscales and changes the wetting properties of the PPy from hydrophilic to hydrophobic over time, which may have potential applications in the biomedical field, energy storage, sensors, adsorption, corrosion resistance, and electromagnetic shielding.

Funding information: The authors gratefully acknowledge the Bu-Ali Sina University for funding this research work. This work was also supported by the Basic Science Research Program through the National Research Foundation of Korea (NRF) funded by the Ministry of Education, Science and Technology (2022R1A2C1004437) and the Korean government (MSIT) (2022M3J7A1062940).

Author contributions: Ensiye Shabanlou: conceptualization, methodology, writing – original draft, writing – review and editing, validation, formal analysis, and investigation. Babak Jaleh: conceptualization, supervision, methodology, writing – original draft, and writing – review and editing. Saeid Azizian: methodology and writing – review and editing. Kyong Yop Rhee: writing – review and editing and support. All authors have accepted responsibility for the entire content of this manuscript and approved its submission.

Conflict of interest: The authors state no conflict of interest.

References

[1] Abd-Elaziem W, Darwish MA, Hamada A, Daoush WM. Titanium-Based alloys and composites for orthopedic implants applications: A comprehensive review. Mater Des. 2024;241:112850.

[2] Kaur M, Singh K. Review on titanium and titanium based alloys as biomaterials for orthopaedic applications. Mater Sci Eng C. 2019;102:844–62.

[3] Gao K, Zhang Y, Yi J, Dong F, Chen P. Overview of surface modification techniques for titanium alloys in modern material science: a comprehensive analysis. Coatings. 2024;14(1):148.

[4] Rikhari B, Saranya K, Kalaiyarasan M, Rahaman M, Periyasami G, Pandiaraj S, et al. Bioactive conductive polymer-coated titanium to support osseointegration. Biomass Convers Biorefin. 2024;14:10699–712.

[5] Al-Shalawi FD, Mohamed Ariff AH, Jung DW, Mohd Ariffin MKA, Seng Kim CL, Brabazon D, et al. Biomaterials as implants in the orthopedic field for regenerative medicine: metal versus synthetic polymers. Polymers. 2023;15(12):2601.

[6] Lorenzetti M, Pellicer E, Sort J, Baró MD, Kovač J, Novak S, et al. Improvement to the corrosion resistance of Ti-based implants using hydrothermally synthesized nanostructured anatase coatings. Materials. 2014;7(1):180–94.

[7] Díaz LA, Cabal B, Prado C, Moya JS, Torrecillas R, Fernández A, et al. High-velocity suspension flame sprayed (HVSFS) soda-lime glass coating on titanium substrate: Its bactericidal behaviour. J Eur Ceram Soc. 2016;36(10):2653–8.

[8] Liao T-Y, King PC, Zhu D, Crawford RJ, Ivanova EP, Thissen H, et al. Surface characteristics and bone biocompatibility of cold-sprayed porous titanium on polydimethylsiloxane substrates. ACS Biomater Sci Eng. 2023;9:1402–21.

[9] Goodarzi S, Moztarzadeh F, Nezafati N, Omidvar H. Titanium dioxide nanotube arrays: A novel approach into periodontal tissue regeneration on the surface of titanium implants. Adv Mater Lett. 2016;7(3):209–15.

[10] Ngaboyamahina E, Cachet H, Pailleret A, Sutter E. Photo-assisted electrodeposition of an electrochemically active polypyrrole layer on anatase type titanium dioxide nanotube arrays. Electrochim Acta. 2014;129:211–21.

[11] El-Shazly A, Wazzan A. Using polypyrrole coating for improving the corrosion resistance of steel buried in corrosive mediums. Int J Electrochem Sci. 2012;7(3):1946–57.

[12] Floroian L, Craciun D, Socol G, Dorcioman G, Socol M, Badea M, et al. Titanium implants' surface functionalization by pulsed laser deposition of TiN, ZrC and ZrN hard films. Appl Surf Sci. 2017;417:175–82.

[13] Shabanlou E, Jaleh B, Mohazzab BF, Kakuee O, Golbedaghi R, Orooji Y. TiN formation on Ti target by laser ablation method under different N_2 gas pressure and laser scanning cycles: A wettability study. Surf Interfaces. 2021;27:101509.

[14] Oyane A, Matsuoka N, Koga K, Shimizu Y, Nakamura M, Kawaguchi K, et al. Laser-assisted biomimetic process for surface functionalization of titanium metal. Colloids Interface Sci Commun. 2015;4:5–9.

[15] Shabanlou E, Jaleh B, Imantalab O, Fattah-Alhosseini A. Corrosion behavior of TiN layer fabricated by laser irradiation of Ti target in N_2/liquid water environment. Ceram Int. 2022;48(18):26934–44.

[16] Mohazzab BF, Jaleh B, Fattah-alhosseini A, Mahmoudi F, Momeni A. Laser surface treatment of pure titanium: Microstructural analysis, wear properties, and corrosion behavior of titanium carbide coatings in Hank's physiological solution. Surf Interfaces. 2020;20:100597.

[17] Mohazzab BF, Jaleh B, Kakuee O, Fattah-Alhosseini A. Formation of titanium carbide on the titanium surface using laser ablation in n-heptane and investigating its corrosion resistance. Appl Surf Sci. 2019;478:623–35.

[18] Garcia-Cabezon C, Garcia-Hernandez C, Rodriguez-Mendez ML, Martin-Pedrosa F. A new strategy for corrosion protection of porous stainless steel using polypyrrole films. J Mater Sci Technol. 2020;37:85–95.

[19] Kanaan AF, Pinho AC, Piedade AP. Electroactive polymers obtained by conventional and non-conventional technologies. Polymers. 2021;13(16):2713.
[20] Pan T, Yu Q. Long-term anti-corrosion performance of a conducting polymer-based coating system for steels. JMEP. 2016;25:2384–94.
[21] Randis R, Darmadi DB, Gapsari F, Sonief AAA, Akpan ED, Ebenso EE. The potential of nanocomposite-based coatings for corrosion protection of metals: A Review. J Mol Liq. 2023;390:123067.
[22] Borges MH, Nagay BE, Costa RC, Souza JGS, Mathew MT, Barão VA. Recent advances of polypyrrole conducting polymer film for biomedical application: Toward a viable platform for cell-microbial interactions. Adv Colloid Interface Sci. 2023;314:102860.
[23] Liang J, Li L, Tong K, Ren Z, Hu W, Niu X, et al. Silver nanowire percolation network soldered with graphene oxide at room temperature and its application for fully stretchable polymer light-emitting diodes. ACS nano. 2014;8(2):1590–600.
[24] Ozdemir M, Choi D, Kwon G, Zorlu Y, Cosut B, Kim H, et al. Solution-processable BODIPY-based small molecules for semiconducting microfibers in organic thin-film transistors. ACS Appl Mater Interfaces. 2016;8(22):14077–87.
[25] Duan X, Deng J, Wang X, Guo J, Liu P. Preparation of polypyrrole nanocomposites for supercapacitor using spent battery powder as raw materials. Electrochim Acta. 2016;210:646–54.
[26] Huang Y, Li H, Wang Z, Zhu M, Pei Z, Xue Q, et al. Nanostructured polypyrrole as a flexible electrode material of supercapacitor. Nano Energy. 2016;22:422–38.
[27] Varghese A., Devi SKR., Kausar F., Pinheiro D. Evaluative study on supercapacitance behavior of polyaniline/polypyrrole–metal oxide based composites electrodes: a review. Mater Today Chem. 2023;29:101424.
[28] Stejskal J, Jurča M, Vilčáková J, Trchová M, Kolská Z, Prokeš J. Conducting polypyrrole silicotungstate deposited on macroporous melamine sponge for electromagnetic interference shielding. Mater Chem Phys. 2023;293:126907.
[29] Lou J, Zhu X, Yang X, Hao H, Ma D, Zhu L, et al. Structure and electrochromic properties of polypyrrole films synthesized by AC electrochemical impedance spectroscopy under different amplitude. Mater Today Commun. 2024;39:108586.
[30] Xiang D, Wang X, Jia C, Lee T, Guo X. Molecular-scale electronics: from concept to function. Chem Rev. 2016;116(7):4318–440.
[31] Wang Z, Cui H, Li S, Feng X, Aghassi-Hagmann J, Azizian S, et al. Facile approach to conductive polymer microelectrodes for flexible electronics. ACS Appl Mater Interfaces. 2021;13(18):21661–8.
[32] Rikhari B, Mani SP, Rajendran N. Investigation of corrosion behavior of polypyrrole-coated Ti using dynamic electrochemical impedance spectroscopy (DEIS). RSC Adv. 2016;6(83):80275–85.
[33] Yu T, Li S, Zhang L, Li F, Pan H, Zhang D. Design and construction of conductive polymer PPy anchored NiCo bi-metal sulfide composite electrode materials for high-performance hybrid supercapacitor and electrochemical hydroquinone sensor. J Energy Storage. 2024;87:111427.
[34] Qi K, Qiu Y, Chen Z, Guo X. Corrosion of conductive polypyrrole: Galvanic interactions between polypyrrole and metal substrates. Corros Sci. 2015;91:272–80.
[35] Wang S, Chen Y, Hu B, Wang Y, Jing X, Li Y. Polypyrrole micro/nanostructures and their soft materials in versatile forms: construction and applications. Mater Chem Front. 2024;8(2):434–54.
[36] Kim YK, Shin K-Y. Dopamine-assisted chemical vapour deposition of polypyrrole on graphene for flexible supercapacitor. Appl Surf Sci. 2021;547:149141.
[37] Lee S, Park CH. Conductivity, superhydrophobicity and mechanical properties of cotton fabric treated with polypyrrole by in-situ polymerization using the binary oxidants ammonium Peroxodisulfate and ferric chloride. Text Res J. 2019;89(12):2376–94.
[38] Negarestani M, Shayesteh H, Kheradmand A, Pahlevani F, Mollahosseini A, Javanshir S. Preparation of polypyrrole-functionalized recycled cotton fiber as a renewable and eco-friendly cellulose-based adsorbent for water decolorization: Comprehensive batch and fixed-bed column study. Surf Interfaces. 2024;48:104360.
[39] Tsumura Y, Fameau A-L, Matsui K, Hirai T, Nakamura Y, Fujii S. Photo-and thermoresponsive liquid marbles based on fatty acid as phase change material coated by polypyrrole: from design to applications. Langmuir. 2023;39(2):878–89.
[40] Kumar AM, Rajendran N. Electrochemical aspects and in vitro biocompatibility of polypyrrole/TiO_2 ceramic nanocomposite coatings on 316L SS for orthopedic implants. Ceram Int. 2013;39(5):5639–50.
[41] Popescu S, Pirvu C, Mindroiu M, Demetrescu I. Enhancing the stability of PPy film on Ti by PEG incorporation. Mol Cryst Liq Cryst. 2010;522(1):125/425.
[42] Rikhari B, Mani SP, Rajendran N. Electrochemical behavior of polypyrrole/chitosan composite coating on Ti metal for biomedical applications. Carbohydr Polym. 2018;189:126–37.
[43] Tan J, Zhang Z, Ge D. Electrodeposition of adherent polypyrrole film on titanium surface with enhanced anti-corrosion performance. The International Conference on Composite Material, Polymer Science and Engineering (CMPSE2017). Vol. 130, EDP Sciences; 2017 Oct 25. p. 08007, MATEC Web Conf.
[44] Luan Y, Jia L, Liu W, Liu P. Nanofibers/reduced graphene oxide/polypyrrole for High-performance electrode material. NPPRJ. 2024;39(1):53–60.
[45] Popescu S, Ungureanu C, Albu AM, Pirvu C. Poly (dopamine) assisted deposition of adherent PPy film on Ti substrate. Prog Org Coat. 2014;77(11):1890–900.
[46] Fomo G, Waryo T, Feleni U, Baker P, Iwuoha E. Electrochemical polymerization. In Functional Biopolymers. Cham, Switzerland: Springer; 2019. p. 105–31.
[47] Wang C, Wang Y, Song X, Huang M, Jiang H. A facile and general strategy to deposit polypyrrole on various substrates for efficient solar-driven evaporation. Adv Sustainable Syst. 2019;3(1):1800108.
[48] Asatekin A, Barr MC, Baxamusa SH, Lau KK, Tenhaeff W, Xu J, et al. Designing polymer surfaces via vapor deposition. Mater Today. 2010;13(5):26–33.
[49] Ahmmed KT, Grambow C, Kietzig A-M. Fabrication of micro/nano structures on metals by femtosecond laser micromachining. Micromachines. 2014;5(4):1219–53.
[50] Wang W, Li PF, Xie R, Ju XJ, Liu Z, Chu LY. Designable Micro-/Nano-Structured Smart Polymeric Materials. Adv Mater. 2022;34(46):2107877.
[51] Ahmadipour M, Arjmand M, Ain MF, Ahmad ZA, Pung S-Y. Effect of Ar: N_2 flow rate on morphology, optical and electrical properties of CCTO thin films deposited by RF magnetron sputtering. Ceram Int. 2019;45(12):15077–81.
[52] El-Khawaga AM, Zidan A, Abd El-Mageed AI. Preparation methods of different nanomaterials for various potential applications: A review. J Mol Struct. 2023;1281:135148.
[53] Augustine S, Sooraj K, Saini M, Hans S, Parida BK, Pachchigar V, et al. SERS sensing of Metanil yellow in turmeric solution using self-organized nanoparticle arrays grown on Ion beam patterned soda-lime glass. Photonics Nanostruct-Fundam Appl. 2023;56:101166.

[54] Lasagni AF. Laser interference patterning methods: Possibilities for high-throughput fabrication of periodic surface patterns. Adv Opt Technol. 2017;6(3–4):265–75.
[55] Toosi SF, Moradi S, Hatzikiriakos SG. Fabrication of micro/nano patterns on polymeric substrates using laser ablation methods to control wettability behaviour: a critical review. Rev Adhes Adhes. 2017;5(1):55–78.
[56] Duta L, Stan GE, Popa AC, Husanu MA, Moga S, Socol M, et al. Thickness influence on in vitro biocompatibility of titanium nitride thin films synthesized by pulsed laser deposition. Mater. 2016;9(1):38.
[57] Estrada-Martínez J, Reyes-Gasga J, García-García R, Vargas-Becerril N, Zapata-Torres MG, Gallardo-Rivas NV, et al. Wettability modification of the AISI 304 and 316 stainless steel and glass surfaces by titanium oxide and titanium nitride coating. Surf Coat Technol. 2017;330:61–70.
[58] Gao C, Qu N. Electrolysis-assisted recovery of superhydrophilicity from superhydrophobized surfaces. Surf Coat Technol. 2019;372:343–52.
[59] Lu J, Huang T, Liu Z, Zhang X, Xiao R. Long-term wettability of titanium surfaces by combined femtosecond laser micro/nano structuring and chemical treatments. Appl Surf Sci. 2018;459:257–62.
[60] Zhou X, Yu S, Guan S, Lv Z, Liu E, Zhao Y. Fabrication and characterization of superhydrophobic TiO_2 nanotube coating by a facile anodic oxidation approach. Surf Coat Technol. 2018;354:83–91.
[61] Höche D, Schikora H, Zutz H, Queitsch R, Emmel A, Schaaf P. Microstructure of TiN coatings synthesized by direct pulsed Nd: YAG laser nitriding of titanium: Development of grain size, microstrain, and grain orientation. Appl Phys A. 2008;91:305–14.
[62] Vangolu Y, Yurtcan MT. Wear and corrosion properties of wollastonite and boron nitride doped, hydroxyapatite-based HAp-Wo-BN composite coatings prepared by pulsed laser deposition. Ceram Int. 2021;47(23):32969–78.
[63] Exir H, Weck A. Mechanism of superhydrophilic to superhydrophobic transition of femtosecond laser-induced periodic surface structures on titanium. Surf Coat Technol. 2019;378:124931.
[64] Razi S, Mollabashi M, Madanipour K. Laser processing of metallic biomaterials: An approach for surface patterning and wettability control. Eur Phys J Plus. 2015;130:1–12.
[65] Liu Z, Niu T, Lei Y, Luo Y. Metal surface wettability modification by nanosecond laser surface texturing: A review. Biosurf Biotribol. 2022;8(2):95–120.
[66] Wenzel RN. Resistance of solid surfaces to wetting by water. Ind Eng Chem. 1936;28(8):988–94.
[67] Fowkes FM. Attractive forces at interfaces. Ind Eng Chem. 1964;56(12):40–52.
[68] Lota K, Acznik I, Sierczynska A, Lota G. Enhancing the performance of polypyrrole composites as electrode materials for supercapacitors by carbon nanotubes additives. J Appl Polym Sci. 2020;137(28):48867.
[69] Ungureanu C, Popescu S, Purcel G, Tofan V, Popescu M, Sălăgeanu A, et al. Improved antibacterial behavior of titanium surface with torularhodin–polypyrrole film. Mater Sci Eng C. 2014;42:726–33.
[70] Sanches EA, Alves SF, Soares JC, da Silva AM, da Silva CG, de Souza SM, et al. Nanostructured polypyrrole powder: a structural and morphological characterization. J Nanomater. 2015;2015:1–8.
[71] Tuschel D. Raman spectroscopy and polymorphism. Spectroscopy. 2019;34:10–21.
[72] Liu B-W, Mi G-Y, Wang C-M. Reoxidation process and corrosion behavior of TA15 alloy by laser ablation. Rare Met. 2021;40:865–76.
[73] Takada N, Sasaki T, Sasaki K. Synthesis of crystalline TiN and Si particles by laser ablation in liquid nitrogen. Appl Phys A. 2008;93:833–6.
[74] Liu Y-C. Characteristics of vibration modes of polypyrrole on surface-enhanced Raman scattering spectra. J Electroanal Chem. 2004;571(2):255–64.
[75] Šetka M, Calavia R, Vojkůvka L, Llobet E, Drbohlavová J, Vallejos S. Raman and XPS studies of ammonia sensitive polypyrrole nanorods and nanoparticles. Sci Rep. 2019;9(1):8465.
[76] Stejskal J, Trchová M, Bober P, Morávková Z, Kopecký D, Vrňata M, et al. Polypyrrole salts and bases: superior conductivity of nanotubes and their stability towards the loss of conductivity by deprotonation. RSC Adv. 2016;6(91):88382–91.
[77] Xie Y, Wang D. Supercapacitance performance of polypyrrole/titanium nitride/polyaniline coaxial nanotube hybrid. J Alloy Compd. 2016;665:323–32.
[78] Malitesta C, Losito I, Sabbatini L, Zambonin P. New findings on polypyrrole chemical structure by XPS coupled to chemical derivatization labelling. J Electron Spectrosc Relat Phenom. 1995;76:629–34.
[79] Dianatdar A, Miola M, De Luca O, Rudolf P, Picchioni F, Bose RK. All-dry, one-step synthesis, doping and film formation of conductive polypyrrole. J Mater Chem C. 2022;10(2):557–70.
[80] Luhakhra N, Tiwari SK. Polaron and bipolaron mediated photocatalytic activity of polypyrrole nanoparticles under visible light. Colloids Surf A: Physicochem Eng Asp. 2023;667:131380.
[81] Feng M, Lu W, Zhou Y, Zhen R, He H, Wang Y, et al. Synthesis of polypyrrole/nitrogen-doped porous carbon matrix composite as the electrode material for supercapacitors. Sci Rep. 2020;10(1):15370.
[82] Cao J, Wang Y, Chen J, Li X, Walsh FC, Ouyang J-H, et al. Three-dimensional graphene oxide/polypyrrole composite electrodes fabricated by one-step electrodeposition for high performance supercapacitors. J Mater Chem A. 2015;3(27):14445–57.
[83] Ullah H. Inter-molecular interaction in Polypyrrole/TiO_2: A DFT study. J Alloy Compd. 2017;692:140–8.
[84] Ullah H, Tahir AA, Mallick TK. Polypyrrole/TiO_2 composites for the application of photocatalysis. Sens Actuators B: Chem. 2017;241:1161–9.
[85] Bakhtiari N, Azizian S, Mohazzab BF, Jaleh B. One-step fabrication of brass filter with reversible wettability by nanosecond fiber laser ablation for highly efficient oil/water separation. Sep Purif Technol. 2021;259:118139.
[86] Fernández-Arias M, Boutinguiza M, del Val J, Riveiro A, Rodríguez D, Arias-González F, et al. Fabrication and deposition of copper and copper oxide nanoparticles by laser ablation in open air. Nanomater. 2020;10(2):300.
[87] Páramo-Garcia U, Avalos-Perez A, Guzman-Pantoja J, Díaz-Zavala NP, Melo-Banda JA, Gallardo-Rivas NV, et al. Polypyrrole microcontainer structures and doughnuts designed by electrochemical oxidation: an electrochemical and scanning electron microscopy study. E-Polym. 2014;14(1):75–84.
[88] Li Y, Tian Y, Yang C, Zhang D, Liu X. Laser-induced hydrophobicity on Ti-6Al-4V surface. Proceedings in: IEEE 3M-NANO - 5th IEEE; International Conference on Manipulation, Manufacturing and Measurement on the Nanoscale (3M-NANO). Changchun, China: 2015 Oct 5–9. p. 153–8.

[89] Žemaitis A, Mimidis A, Papadopoulos A, Gečys P, Račiukaitis G, Stratakis E, et al. Controlling the wettability of stainless steel from highly-hydrophilic to super-hydrophobic by femtosecond laser-induced ripples and nanospikes. RSC Adv. 2020;10(62):37956–61.
[90] Idla K, Inganäs O, Strandberg M. Good adhesion between chemically oxidised titanium and electrochemically deposited polypyrrole. Electrochim Acta. 2000;45:2121–30.
[91] De Giglio E, Guascito MR, Sabbatini L, Zambonin G. Electropolymerization of pyrrole on titanium substrates for the future development of new biocompatible surfaces. Biomater. 2001;22(19):2609–16.
[92] Jacques A, Barthélémy B, Delhalle J, Mekhalif Z. 1-Pyrrolyl-10-decylammoniumphosphonate monolayer: a molecular nanolink between electropolymerized pyrrole films and nickel or titanium surfaces. Electrochim Acta. 2015;170:218–28.
[93] Liao Q, Hou H, Duan J, Liu S, Yao Y, Dai Z, et al. Composite sodium p-toluenesulfonate/polypyrrole/TiO_2 nanotubes/Ti anode for sodium ion battery. Int J Hydrog Energy. 2017;42(17):12414–9.
[94] Chen L, Mou S, Li F, Zeng Y, Sun Y, Horch RE, et al. Self-assembled human adipose-derived stem cell-derived extracellular vesicle-functionalized biotin-doped polypyrrole titanium with long-term stability and potential osteoinductive ability. ACS Appl Mater Interfaces. 2019;11(49):46183–96.
[95] Rikhari B, Mani SP, Rajendran N. Polypyrrole/graphene oxide composite coating on Ti implants: A promising material for biomedical applications. J Mater Sci. 2020;55(12):5211–29.
[96] Rasouli H, Hosseini MG, Yardani Sefidi P, Kinayyigit S. Superior overall water splitting performance in polypyrrole photoelectrode by coupling NrGO and modifying electropolymerization substrate. J Appl Polym Sci. 2021;138(21):50507.
[97] Rasouli H, Hosseini MG, Hosseini MM. Ta_2O_5-incorporated in photoinduced electrocatalyst of TiO_2-RuO_2 decorated by PPy-NrGO nanocomposite for boosting overall water splitting. J Colloid Interface Sci. 2021;582:254–69.
[98] Borges M, Nagay B, Costa R, Sacramento C, Ruiz K, Landers R, et al. A tattoo-inspired electrosynthesized polypyrrole film: crossing the line toward a highly adherent film for biomedical implant applications. Mater Today Chem. 2022;26:101095.
[99] García-Cabezón C, Godinho V, Pérez-González C, Torres Y, Martín-Pedrosa F. Electropolymerized polypyrrole silver nanocomposite coatings on porous Ti substrates with enhanced corrosion and antibacterial behavior for biomedical applications. Mater Today Chem. 2023;29:101433.